

LBL-20380

c.1

VC-25

LBL-20380

RECEIVED
LAWRENCE
BERKELEY LABORATORY

FEB 18 1986

LIBRARY AND
DOCUMENTS SECTION

HIGH TEMPERATURE STRESS CORROSION
CRACKING IN CERAMICS

H. Cao
(M.S. Thesis)

June 1985

For Reference
Not to be taken from this room

Lawrence Berkeley Laboratory
University of California
Berkeley, California 94720

Prepared for the U.S. Department of Energy
under Contract DE-AC03-76SF00098

CCM

**Center
for
Advanced
Materials**

LBL-20380
c.1

DISCLAIMER

This document was prepared as an account of work sponsored by the United States Government. While this document is believed to contain correct information, neither the United States Government nor any agency thereof, nor the Regents of the University of California, nor any of their employees, makes any warranty, express or implied, or assumes any legal responsibility for the accuracy, completeness, or usefulness of any information, apparatus, product, or process disclosed, or represents that its use would not infringe privately owned rights. Reference herein to any specific commercial product, process, or service by its trade name, trademark, manufacturer, or otherwise, does not necessarily constitute or imply its endorsement, recommendation, or favoring by the United States Government or any agency thereof, or the Regents of the University of California. The views and opinions of authors expressed herein do not necessarily state or reflect those of the United States Government or any agency thereof or the Regents of the University of California.

High Temperature Stress Corrosion
Cracking in Ceramics

Hengchu Cao
M.S. Thesis

Lawrence Berkeley Laboratory
University of California
Berkeley, California 94720

June 1985

This work was supported by the Director, Office of Energy Research, Office of Basic Energy Sciences, Materials Sciences Division of the U.S. Department of Energy under Contract Number DE-AC03-76SF00098.

Table of Contents

	<u>Page</u>
Abstract	v
1. Introduction	1
2. Experimental	2
2.1. Procedures	2
2.2. Observations	4
2.3. Measurements	5
3. Crack Propagation Model.	6
3.1. The Crack Shape.	7
3.2. The Crack Propagation Velocity	10
4. Discussion	13
4.1. Crack Nucleation	13
4.2. Crack Propagation.	13
4.3. Crack Arrest	15
4.4. Creep Rupture.	16
5. Concluding Remarks	18
Acknowledgements	19
References	20
Table	22
Figure Captions.	23
Figures.	25

HIGH TEMPERATURE STRESS CORROSION CRACKING IN CERAMICS

Hengchu Cao
(M.S. Thesis)

Center for Advanced Materials
Lawrence Berkeley Laboratory
and
Department of Materials Science and Mineral Engineering
University of California, Berkeley, CA 94720

Master's of Science Thesis

ABSTRACT

Single phase ceramics are shown to be susceptible to stress corrosion cracking at elevated temperatures in the presence of a wetting amorphous deposit. The effect is demonstrated to involve diffusive crack growth, motivated by the small crack tip dihedral angle induced by the amorphous phase. Crack arrest and subsequent blunting are also shown to occur both when the crack is depleted of amorphous material and when the stress intensity is below the blunting threshold. Implications for stress corrosion induced premature failures are discussed.

1. INTRODUCTION

Ceramics have many advantages over metallic alloys as a class of high temperature structural materials. The recently developed high temperature ceramics, such as ZrO_2 , Si_3N_4 , SiC, sialons and Al_2O_3 , have application in advanced heat engines and nuclear power. The basic understanding of the mechanical behavior of this category of materials is thus very important. The mechanical failure of ceramics at elevated temperatures is believed to involve several sequential processes: cavity nucleation on the grain boundaries, cavity growth, crack nucleation through the coalescence of the cavities and crack propagation [1]. A recent study indicated that creep cracks usually initiate at the material heterogeneities, such as large-grained regions and nickel-enriched regions in hot pressed alumina [2]. Below a threshold stress level, creep cracks are observed to blunt and the shear bands form ahead of the crack tip, inclined to the crack plane. The final failure involves damage development through the shear bands [3].

However, the high temperature mechanical properties of ceramics are also subject to various environmental influences. It has been known for some time that non-oxide ceramics are susceptible to oxidizing environments [4,5], and that such oxidation may result in strength limiting flaws [6,7] as well as continuous microstructural changes that affect both the creep rate and the fracture toughness [8,9]. Additionally, stress corrosion cracking may occur in selected liquid or gaseous media [10]. More recently, it has been demonstrated that oxide ceramics are prone to both microstructural changes in oxidizing

environments [11], and to stress corrosion cracking [2,12]. The mechanisms of the stress corrosion cracking have not yet been well established. The intent of the present study is to establish the characteristics of one important high temperature stress corrosion cracking mechanism.

An experimental investigation of the high temperature mechanical properties of a nominally single phase polycrystalline alumina revealed the existence of premature cracking in the presence of silica or silicate particulates in the test ambient (fig. 1) [2,12]. The cracking was attributed to stress enhanced penetration of the amorphous materials into the grain boundaries, resulting in a localized creep embrittlement [2]. A stress corrosion mechanism is implied. A systematic investigation of this phenomenon is presented in the present thesis. The experimental aspect of the investigation entails placement of an array of silicate spots onto alumina test specimens, followed by application of stress at elevated temperature and observation of the resultant cracking through the scanning electron microscope. A series of interrupted tests enable the crack propagation velocities to be measured at each stage of the stress corrosion cracking. A theoretical analysis of the stress enhanced grain boundary penetration by a wetting amorphous phase is then presented. Finally, a discussion of the effects of the environment on the creep rupture provides insights regarding microstructural and environmental effects on the rupture life.

2. EXPERIMENTAL

2.1. Procedures

Beams of a fine grained hot pressed alumina* having dimensions 30 by 3 by 3 mm were prepared by diamond cutting and polishing. The microstructure and creep characteristics of this material have been described elsewhere [11]. The silicate stress corrosion medium was emplaced onto one surface of the beam using the following procedure. Soda lime silicate glass spheres** having diameters in the range of 5 to 20 μm were suspended in keroscene. Several drops of the suspension were placed onto the beam surface to form a smooth film. When the film was nearly dry, the glass spheres were arranged into the desired array under a binocular optical microscope. The beam was then carefully transferred to a furnace and heated to about 1200°C for 30 minutes. At this temperature the glass spread into circular spots on the specimen surface (fig. 2), with diameters in the range 30 to 80 μm .

Subsequent to emplacement of the stress corrosive medium, the test specimens were subjected to four point flexure at constant stress at temperatures of 1300 to 1400°C. The tests were intercepted at various strain intervals, the specimens cooled to room temperature under load, and the damage characterized in the scanning electron microscope.

* Hot pressed with 1/4 percent magnesia by Arco Corp.

**Minnesota Mining and Manufacturing Company.

2.2. Observations

After relatively small creep strains ($\sim 1\%$), cracks were observed to nucleate at the interface between the amorphous spot and the matrix (fig. 3). At this stage, the cracks were completely filled with amorphous materials, viscously transported along the crack from within the spot. Initially, the cracks continued to grow, with the crack tip remaining sharp (fig. 4). During this period the grains within the spot were subject to appreciable faceting (fig. 4), indicative of rapid mass transport via the amorphous medium. Subsequently, a liquid/vapor meniscus formed between the crack surface (fig. 5) that gradually propagated toward the advancing crack tip. When the meniscus reached the crack tip, crack propagation ceased. Further straining was then accompanied by crack blunting and large crack opening displacement (fig. 6a) without crack extension. Final rupture of the specimens occurs by coalescence of the arrested cracks across intervening shear bands (fig. 6b).

In a few instances, specimens tested to strain just beyond crack initiation were cooled under load and fractured at room temperature. Observations of the fracture surface (fig. 7) revealed that the stress corrosion crack exhibited an approximately semi-circular profile. Furthermore, the stress corrosion crack appeared to be entirely intergranular (fig. 8a) and accompanied by extensive faceting. By contrast the room temperature fracture had both intergranular and transgranular features, with no evidence of faceting (fig. 8c).

2.3 Measurements

Knowledge of the semicircular crack shape allows a stress intensity factor K to be assigned to each surface trace [13]. Consequently, an approximate relation between the crack growth rate v and the stress intensity factor K can be obtained. The results (fig. 9) conform to previous measurements [14] which indicate that the stress corrosion cracks grow relatively rapidly at stress intensities below the threshold, K_{th} , at which creep cracks blunt without propagation.

The radii at which the stress corrosion cracks arrest and blunt, a_a have been measured, and related to the diameter of the associated amorphous spots, b . These measurements reveal that a_a/b is approximately constant (fig. 10) and equal to 3.7.

Finally, the room temperature fracture stress of the specimens tested to strains just beyond the stress corrosion crack initiation strain has been measured. The fractures occur through the stress corrosion cracks and the strengths data are fully consistent with values expected from the crack size and the room temperature toughness (table I).

3. CRACK PROPAGATION MODEL

Rapid crack propagation in the presence of amorphous material results from a dual role of the amorphous phase. The primary effect of the glass apparently derives from its wetting characteristics, which induce a relatively sharp crack tip by virtue of the small dihedral angle ψ_0 at the grain boundary/liquid intersection (fig. 11a), as expressed by;

$$\psi_0 = \cos^{-1} (\gamma_b / 2\gamma_{\ell s}) \quad (1)$$

where γ_b is the grain boundary energy and $\gamma_{\ell s}$ is the energy of the liquid/solid interface. The second influence of the glass is to provide a medium for rapid transport of the solid from the crack surfaces to the crack tip. A suitable crack propagation model would thus consist of a crack growing along a grain boundary by means of liquid phase transport within the crack and grain boundary diffusion in the solid. The simplest geometric situation having these features, illustrated in fig. 11a, represents a model similar to a creep crack growth model previously developed by Chuang and Rice [15] (except that surface diffusion along the crack surfaces is replaced by liquid phase transport within the crack). An approximate analytic treatment of crack growth, having the essential physical features, is presented in this section. Initially, the crack shape is analyzed in order to obtain a solution for the flux through the crack tip. This result is then coupled with a solution for the flux along the grain boundary ahead of the crack [16] to obtain a relation between v and K .

3.1. The Crack Shape

For simplicity, steady-state crack propagation is considered, such that the crack shape remains constant as the crack extends. Furthermore, moving coordinates are used with the crack tip as origin. Assuming that mass transport through the liquid is diffusion (rather than interface) controlled, the concentration c of the alumina in the liquid in contact with the crack surface is related to the local surface curvature, κ , by;

$$\ln (c/c_0) = \gamma_{\ell s} \Omega \kappa / kT \quad (2a)$$

or $(c \sim c_0)$;

$$c \approx c_0 + c_0 \gamma_{\ell s} \kappa \Omega / kT \quad (2b)$$

where Ω is the atomic volume and c_0 is the concentration in equilibrium with a flat surface. For analytic tractability, the concentration gradients in the liquid are referred to annular elements defined by crack surface tangents. Specifically, tangents to the crack surface are drawn to intersect the crack plane, at angle ψ (fig. 11b). Then, with this intersection point as origin, the angular segment (r, ψ) defines a region within which, at steady state (c independent of time in the moving coordinates), the Laplace equation is satisfied, [17]

$$\frac{\partial^2 c}{\partial \rho^2} + \frac{1}{\rho} \frac{\partial c}{\partial \rho} + \frac{1}{\rho^2} \frac{\partial^2 c}{\partial \phi^2} = 0 \quad (3)$$

where (ρ, ϕ) are coordinates within the element (r, ψ) , as depicted in fig. 11b.

Furthermore, for small deviations from equilibrium, the boundary condition on the crack surface ($\phi = \psi$) is obtained from eq. (2) as

$$\frac{dc}{d\rho} = \frac{c_0 \gamma_{\ell s} \Omega}{kT} \frac{d\kappa}{ds}$$

where ds is an element of the surface; while on the central plane ($\phi = 0$), symmetry requires that $dc/d\phi = 0$. The solution to the eqn. (3) with the appropriate properties and subject to these boundary conditions is;

$$c/c_0 = 1 + \frac{\gamma_{\ell s} \Omega}{kT} \left\{ \kappa + r \frac{d\kappa}{ds} \left(1 - \frac{r \cos \phi}{\rho \cos \psi} \right) \right\}. \quad (4)$$

Mass conservation imposed on the matter entering each element of liquid from the moving crack surface dictates that

$$\frac{v \sin \psi ds}{\Omega} = D \left[\frac{\partial c}{\rho \partial \phi} \right]_{\rho=r}$$

where D is the diffusivity of the solid in the liquid and v is the crack velocity. Hence, by noting that $dx = ds \cos \psi$, we obtain,

$$\frac{d\kappa}{dx} = \frac{v k T}{\Omega^2 D c_0 \gamma_{\ell s}} \quad (5)$$

where (x, y) are moving cartesian coordinates with origin at the crack tip. Furthermore, since the curvature is given by

$$\kappa \equiv y'' [1 + (y')^2]^{-3/2}$$

eqn. (5) can be re-expressed as;

$$\frac{d^2 G}{dX^2} = 1 \quad (6)$$

where $G = y' (1 + (y')^2)^{-1/2}$, and $X = (vkT/\Omega^2 D c_0 \gamma_{\ell s})^{1/2} x$ (such that $\kappa = dG/dx$). The crack shape can be solved from eqn. (6) by noting that the crack surfaces become planar at some distance X_0 behind the crack tip, whereupon the gradient and the curvature of the surface satisfy

(at $X = X_0$), $G = dG/dX = 0$. Then the solution to eqn. (6) becomes,

$$2G = (X_0 - X)^2 \quad (7)$$

or,

$$\frac{dY}{dX} = \frac{(X_0 - X)^2}{2(1 - (X_0 - X)^4/4)^{1/2}}$$

where $Y = (vkT/\Omega^2 Dc_0 \gamma_{ls})^{1/2} y$ and $dy/dx = dY/dX$. At the crack tip, $X = 0$ and $G = \sin \psi_0$, and thus,

$$X_0 = \sqrt{2} [1 - (\gamma_b/2 \gamma_{ls})^2]^{1/4}. \quad (8)$$

Integration of eqn. (7) gives;

$$Y = H - 2 \int_0^{(X_0 - X)/\sqrt{2}} \frac{t^2}{\sqrt{1 - t^4}} dt \quad (9)$$

where

$$H = \sqrt{2} \int_0^{X_0/\sqrt{2}} \frac{t^2}{\sqrt{1 - t^4}} dt$$

is the normalized crack thickness (at $X = X_0$), plotted as a function of γ_b/γ_{ls} (or ψ_0) in fig. 12. Evidently, the crack thickness decreases as the dihedral angle becomes smaller. Typical crack shapes predicted by eqn. (9) are plotted in fig. 13. Note that, when the dihedral angle $\psi_0 < \pi/12$, eqn. (9) can be approximated (within 5 percent) by;

$$Y \approx [X_0^3 - (X_0 - X)^3]/6 \quad (10)$$

such that $H \approx X_0^3/6 \equiv (\sqrt{2}/3) [1 - (\gamma_b/2 \gamma_{ls})^2]^{3/4}$.

The concentration gradients in the liquid corresponding to the crack shapes depicted fig. 13 are plotted in fig. 14. These gradients reveal that crack growth must proceed by solid being drawn from the liquid at the crack tip into the adjacent grain boundary. A flux of solid thereby occurs within the liquid, toward the crack tip, maintained by dissolution of the solid from the crack surfaces. The atom flux into the crack tip that motivates crack growth is given by;

$$J_{\text{tip}} = \frac{2hv}{\Omega} = \frac{2Hv}{\Omega} \left(\frac{\Omega^2 D \gamma_{\ell s} c_0}{v k T} \right)^{1/2}$$

$$\approx \frac{2\sqrt{2}}{3} \left(\frac{D \gamma_{\ell s} c_0 v}{k T} \right)^{1/2} [1 - (\gamma_b/2 \gamma_{\ell s})^2]^{3/4} \quad (11)$$

The corresponding crack curvature at the tip is;

$$\kappa_{\text{tip}} = -\sqrt{2} \left(\frac{v k T}{\Omega^2 D \gamma_{\ell s} c_0} \right)^{1/2} [1 - (\gamma_b/2 \gamma_{\ell s})^2]^{1/4} \quad (12)$$

The quantities κ_{tip} and J_{tip} can be used in conjunction with a separate solution for the flux along the grain boundary, at the crack tip, to solve the crack velocity as a function of the stress intensity factor K .

3.2. The Crack Propagation Velocity

The grain boundary flux for a semi-infinite crack extending along an elastic bicrystal has previously been solved by Chuang [16]. This solution can be expressed as;

$$K = \sqrt{2\pi} [0.24 \sigma_0' L^{3/2} + 0.30 \sigma_0 L^{1/2}] \quad (13)$$

where σ_0 and σ_0' are the stress and stress gradient at the crack

tip, respectively and

$$L = \left[\frac{\pi E D_b \sigma_b}{4 (1 - \nu^2) k T \nu} \right]^{1/2} \quad (14)$$

where E is the Young's modulus, ν is Poisson's ratio and $D_b \delta_b$, is the grain boundary diffusivity. However, the stress terms are explicitly related to the crack tip curvature and the flux (eqns. 11 and 12), such that

$$\begin{aligned} \sigma_o &\equiv - \kappa_{tip} \gamma_{\ell s} \\ &= \sqrt{2} [1 - (\gamma_b/2 \gamma_{\ell s})^2]^{1/4} \left(\frac{c_o \gamma_{\ell s} \Omega^2 D}{\nu k T} \right)^{1/2} \gamma_{\ell s} \end{aligned} \quad (15a)$$

and

$$\begin{aligned} \sigma_o' &\equiv k T J_{tip} / D_b \delta_b \\ &= \frac{2\sqrt{2} k T}{3 D_b \delta_b} \left(\frac{\nu D \gamma_{\ell s} c_o k T}{\Omega} \right)^{1/2} [1 - (\gamma_b/2 \gamma_{\ell s})^2]^{3/4} \end{aligned} \quad (15b)$$

The crack velocity, above a threshold K_m , level is thus;

$$\frac{K}{K_m} = \frac{1}{2} \left[\left(\frac{\nu}{\nu_m} \right)^{1/4} + \left(\frac{\nu}{\nu_m} \right)^{-1/4} \right], \quad (16)$$

where

$$K_m = 1.4 \left(\frac{E \gamma_{\ell s}}{1 - \nu^2} \right)^{1/2} \left(\frac{D c_o \gamma_{\ell s} \Omega}{k T} \right)^{1/2} [1 - (\gamma_b/2 \gamma_{\ell s})^2]^{1/2}$$

and

$$\nu_m = \frac{0.22 E k T}{(1 - \nu^2) \Omega^2 D_b \delta_b \gamma_{\ell s}} [1 - (\gamma_b/2 \gamma_{\ell s})^2].$$

When the dihedral angle ψ_0 approaches zero (perfect wetting), the threshold K also approaches zero and eqn. (16) can be approximated by;

$$v \approx \frac{K^4 k T (1 - v^2)}{\sin \psi_0 \Omega^2 D_b \delta_b E} \quad (17)$$

The important influence of the wetting characteristics, ψ_0 , on the crack velocity is thus immediately evident. Trends in crack velocity for various ψ_0 are plotted on fig. 9 for comparison with the experimental results. Whereas the comparison seems reasonable, it is noted the present Al_2O_3 material should be regarded as a viscoelastic (rather than elastic) solid. The constraining stress ahead of the crack thus relaxes with time (velocity) causing the crack to extend more rapidly than predicted by the present analysis. The viscoelastic aspects of the problem remain to be studied.

4. DISCUSSION

Several aspects of the stress corrosion cracking problem are addressed by the present study: crack nucleation, crack growth and crack arrest. These phenomena are discussed separately and then evaluated with reference to the presence of stress corrosive species in the environment.

4.1. Crack Nucleation

The observation that cracks nucleate at the interface between the matrix and the amorphous deposit (fig. 3) implies that the nucleation is assisted by stress concentration. Specifically, the region infiltrated by the amorphous material evidently has a lower viscosity than the matrix, owing to relatively rapid mass transport of the solid through the amorphous phase, as manifest in the rapid facetting of the grains (fig. 4). The low viscosity results in stress concentrations, within the matrix, around the amorphous zone [11]. It is presumed that these stress concentrations preferentially motivate penetration of the amorphous phase into selected grain boundaries of the matrix, at the amorphous zone periphery, and thereby nucleate cracks. However, detailed analysis of nucleation process is beyond the scope of this thesis.

4.2. Crack Propagation

It is evident from the present observations that the stress corrosion cracks propagate readily along grain boundaries. Furthermore, the crack growth model presented in section 3 indicates that such propagation can proceed by liquid phase transport of the solid from the

crack surface into the crack tip, in series with grain boundary diffusion (as motivated by the stress gradient ahead of the crack [16]). This behavior deviates appreciably from that observed in single phase materials [3]. Creep crack growth in such materials requires development of a zone of damage (manifest as cavities) ahead of the crack, such that crack growth occurs by coalescence of damage in the crack tip field (fig. 15a). Such cavitation damage is not observed in association with stress corrosion cracking (fig. 4, 8).

The major change in crack growth mechanism induced by the amorphous material is attributed to the substantial reduction in dihedral angle, ψ_0 , provided by the amorphous phase. The essential dihedral angle phenomenon is illustrated in fig. 15, and refers to the material response when the crack reaches a grain triple junction. In the absence of liquid, ψ_0 is large, $\sim 60^\circ$. For this case, extension of the crack by mass transport from the crack surface into the adjoining grain boundaries, subject to force equilibrium at the crack tip, requires crack shape changes (at least when the surface diffusivity is relatively high) involving extensive matter removal from the crack surface. Analysis of this process is complex, due to the transient nature of the crack surface profile; nevertheless the essential features can be adequately illustrated by means of a schematic diagram (fig. 15b). It is believed that the triple junction restriction on diffusive crack propagation is the origin of the damage zone mechanism exhibited by creep crack in single phase materials [18] (fig. 15a).

When a wetting liquid is present at the crack tip, the triple junction represents a less restrictive obstacle to crack growth by matter transport. Specifically, the small dihedral angle permits propagation of very narrow cracks, which may develop a 'steady-state' shape with minimal crack extension beyond the triple junction (fig. 15c). Hence, relatively small matter fluctuations permit continued growth of the crack along an adjoining grain boundary. The elimination of the triple point restriction is believed to occur when $\psi_0 \sim 30^\circ$, because the crack surface at the apex of the junction then remains convex when matter fluctuation occurs at the junction.

Subject to the occurrence of this mechanism transition, in the presence of the amorphous phase, trends in the crack velocity are adequately described by eqns. (16). Notably, the threshold stress intensity diminishes and the crack velocity increases as the dihedral angle approaches zero. This trend is seeming consistent with the present crack growth data (fig. 9), albeit the viscoelastic aspects of crack growth remain to be incorporated.

4.3. Crack Arrest

The experimental observations suggest that crack arrest is associated with a depletion of the amorphous material, due to its deposition on the surfaces of the extending crack. Notably, when liquid is no longer available to the crack tip, the triple junction restriction (fig. 15b) operates, and the crack can only propagate when a damage mechanism is available, (at $K > K_{th}$).

By assuming that none of the amorphous material is lost by evaporation, the crack arrest length a_a due to liquid depletion can be related to the spot radius, b . This is achieved by equating the volume of the amorphous sphere to the volume of the amorphous material on the crack surfaces. For this purpose, it is presumed that the liquid spreads over the surface to form a thin film of thickness, t . Then the spot radius, b , is related to the original sphere volume, V , by,

$$V = \pi b^2 t. \quad (18)$$

Similarly, if the liquid were fully deposited on the crack surfaces with thickness, δ , then;

$$V = \pi a_a^2 \delta$$

whereupon,

$$a_a/b \approx t/\delta = \text{constant}. \quad (19)$$

A constant ratio, a_a/b , is in fact observed (fig. 10), albeit eqn. (19) is regarded as highly approximate, since a significant fraction of the amorphous phase must remain between the alumina grains within the region of the original spot.

4.4 Creep Rupture

When either the stress σ , or the amorphous spot radius b are relatively large, the crack arrest stress intensity, $K_a \approx (2/\sqrt{\pi}) \sigma \sqrt{3.7b}$, may exceed the blunting threshold, K_{th} . Further crack growth may then proceed by the damage zone mechanism and very short creep rupture life would ensue. Stress corrosion enhanced premature ruptures are thus expected in certain instances, substantially debilitating the high temperature utility of the material. Such failures can be

averted by requiring that the amorphous phase deposition be small, such that $K_a < K_{th}$, whereupon

$$b < \frac{\pi}{14.8} \left(\frac{K_{th}}{\sigma} \right)^2. \quad (20)$$

This inequality represents a useful preliminary criterion for avoiding premature rupture.

When $K < K_{th}$, present evidence suggests that creep rupture occurs by shear band coalescence. Furthermore, the rupture strain is not appreciably different from that obtained in the absence of stress corrosion cracks (fig. 16). Hence, such cracks do not appear to be especially detrimental in this failure regime, despite their role as shear band origins. Additional understanding of this behavior is required, based on further studies of shear band failures.

5. CONCLUDING REMARKS

A stress corrosion cracking mechanism for single phase ceramics at elevated temperatures has been established through both experimental investigation and theoretical analysis. The cracking occurs in three stages: crack nucleation, crack propagation and crack arrest. It is shown that the nucleation phase is relatively short, because the amorphous spot on the surface gives rise to a creep strain concentration. Upon nucleation, the crack is filled up with amorphous material, which enhances the mass transport process, and causes the crack to propagate at a velocity $\propto K^4$. Once the amorphous phase is depleted, cracks are observed to arrest and blunt. Crack growth without an amorphous phase occurs by damage coalescence.

The present model requires additional development. First, the dissolution of the solid into the amorphous phase may become the rate limiting process, when the diffusion coefficient of the solid through the amorphous phase becomes relatively large. This usually occurs when the service temperature becomes greater than the glass transition temperature. Second, the material response to the stress should be described by a viscoelastic model.

Acknowledgement

I wish to express my gratitude to Professor Anthony G. Evans for his continuous guidance and encouragement. Thanks are also extended to Professors Lutgard C. DeJonghe and David B. Bogy for their careful review and valuable comments on the thesis. Among other colleagues, I am appreciative to Dr. Brian J. Dalgleish for his help in carrying out the experiments. Finally, I take this opportunity to express my deepest love and appreciation to my late parents for their love and understanding, without which this thesis could not have been done.

This work was supported by the Director, Office of Basic Energy Science, Materials Science Division of the U. S. Department of Energy under Contract No. DE-AC03-76SF00098.

REFERENCES

1. Evans, A. G.—"Creep and Fracture of Engineering Materials and Structures," (ed. Wilshire, B. and Owen, D. R. J.), p. 53. Pineridge Press, Swansea.
2. Evans, A. G. and Blumenthal, W.—"Deformation of Ceramics II," (ed. Tressler, R. E. and Bradt, R. C.), p. 487. Plenum Publishing Corp.
3. Dalglish, B. J. and Evans, A. G., J. Am. Ceram. Soc., 68 [1]44-48 (1985).
4. Singhal, S. C., "Oxidation Kinetics of Hot-Pressed Silicon Carbide," J. Mater. Sci., 11 [7] 1246-53 (1976).
5. Heuer, A. H., Ogbuji, L. U. and Mitchell, T. E., "The Microstructure of Oxide Scales on Oxidized Si and SiC Single Crystals," J. Am. Ceram. Soc., 63 [5-6] 354-5 (1980).
6. Tighe, N. J., "The Structure of Slow-Crack Interfaces in Silicon Nitride," J. Mater. Sci., 13 p. 1455 (1978).
7. Minford, E., et al., "Oxidation Effects on Crack Growth and Blunting in SiC Ceramics," in FRACTURE MECHANICS OF CERAMICS, (ed. Bradt, R. C. and Evans, A. G.), p. 511, vol. 6, Pleunum Publishing Corp.
8. Singhal, S. C. and Lange, F. F., "Effect of Alumina Content on the Oxidation of Hot-Pressed Silicon Carbide," J. Am. Ceram. Soc., 58 [9-10] 433-35 (1975).
9. Tighe, N. J. and Wiederhorn, S. M., "Effects of Oxidation on the Reliability of Silicon Nitride," in FRACTURE MECHANICS OF CERAMICS, (ed. Bradt, R. C., et al.), vol. 5, p. 403, Pleunum Publishing Corp.

10. Kossowsky, R., "Creep and Fatigue of Si_3N_4 as Related to Microstructures in Ceramics for High Performance Applications II," (ed. Burke, J. J. et al.), Brook Hill, MA. 1974.
11. Dalglish, B. J., Johnson, S. M., and Evans, A. G., "High Temperature Failure of Polycrystalline Alumina: I, Crack Nucleation," J. Am. Ceram. Soc. 67 [11] 741-50, 1984.
12. Blumenthal, W. and Evans, A. G., "High Temperature Failure of Polycrystalline Alumina: II, Creep Crack Growth and Blunting," J. Am. Ceram. Soc. 67 [11] 751-59, 1984.
13. Rooke, D. P., "Compendium of Stress Intensity Factors," (ed. Cartwright, D. J.), Her Majesty's Stationery Office, Hillingdon Press, Oxbridge, 1976, p. 299.
14. Blumthal, W., Ph.D. Thesis, University of California, Berkeley, 1983.
15. Chuang, T. J. and Rice, J. R., "The Shape of Intergranular Creep Cracks Growing by Surface Diffusion," Acta. Metall. 21 [12] 1625-28, (1973).
16. Chuang, T. J. "A Diffusive Crack-Growth Model for Creep Fracture," J. Am. Ceram. Soc. 65 [2] 93-103, 1982.
17. Shewman, P. G., DIFFUSION IN SOLIDS, McGraw-Hill Book Company.
18. Thouless, M. D., Hsueh, C. H. and Evans, A. G., "A Damage Model of Creep Crack Growth in Polycrystals," Acta. Metall. 31 [10] 1075-87 (1983).

TABLE I

Failure of Specimens at Room Temperature After
Exposure to Stress Corrosion at Elevated Temperature

Failure Stress (MPa)	Crack Size (μm)	Critical Stress intensity, K_{IC} ($\text{MPa}\sqrt{\text{m}}$)
270	143	2.7
228	168	2.5

Note: Surface crack measurements of K_{IC} at room temperature give,

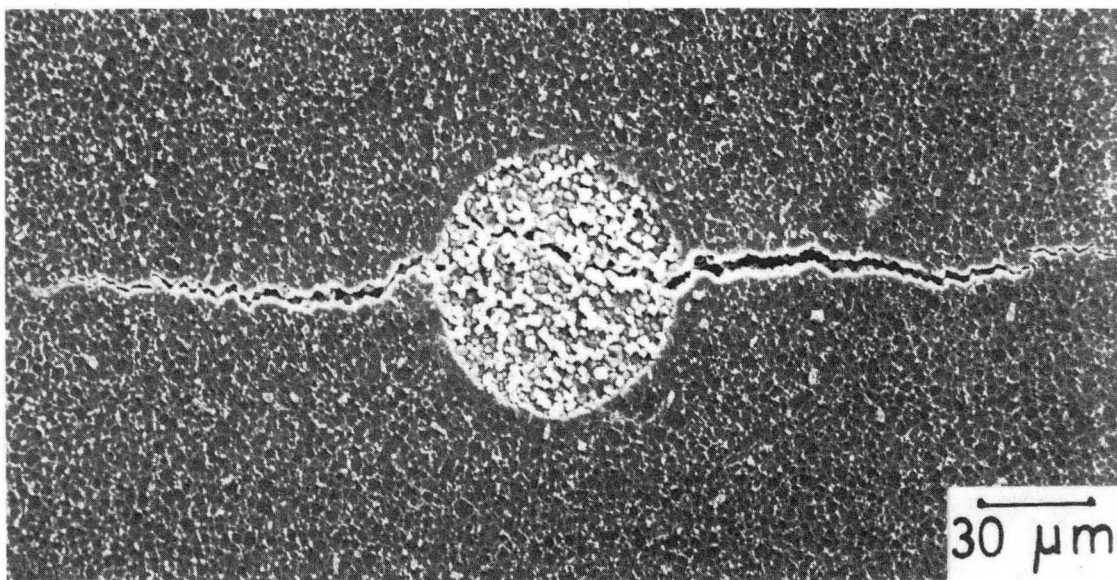
$$K_{IC} = 2.0 \pm 0.4 \text{ MPa}\sqrt{\text{m}}.$$

FIGURE CAPTIONS

- Fig. 1. SEM micrograph of a stress corrosion crack in Al_2O_3 .
- Fig. 2. Circular glass spot on the specimen surface.
- Fig. 3. Crack nucleation at the interface between the amorphous spot and the matrix.
- Fig. 4. Sharp crack filled with glassy phase and faceting of the grains within the glass spot.
- Fig. 5. Liquid/vapor meniscus (marked A) formation between the crack surfaces, after the crack has been subject to appreciable propagation.
- Fig. 6. a) Crack blunting and crack surface widening, followed by;
b) Shear band formation.
- Fig. 7. Fracture surface revealing the semicircular shapes of the stress corrosion crack.
- Fig. 8. a) Grain surface faceting accompanying stress corrosion cracking;
b) Meniscus structure along the crack front trace;
c) Mixed transgranular and intergranular brittle fracture.
- Fig. 9. The velocity of stress corrosion cracks compared with creep crack growth rates. Also shown are predictions of the present model for various values of the dihedral angle.
- Fig. 10. Relation between the length of the arrested stress corrosion cracks and the radii of the associated amorphous spots.

- Fig. 11. a) Schematic of stress corrosion crack geometry and flux;
b) Schematic of an annular element within which time independent mass transport occurs.
- Fig. 12. Trends in normalized crack thickness with dihedral angle.
- Fig. 13. Typical crack shapes for different dihedral angles ψ_0 ,
calculated from equation (9).
- Fig. 14. Typical concentration gradients within the liquid, up to the
crack tip.
- Fig. 15. Schematic illustrating triple junction effects during creep
crack growth:
- a) A damage mechanism of crack growth;
 - b) Diffusive crack growth without damage for large dihedral
angle;
 - c) Diffused crack growth without damage for small dihedral
angle induced by an amorphous phase within the crack.
- Fig. 16. Creep rupture data compared with results obtained in the
absence of a stress corrosion medium.

\uparrow σ_{∞}

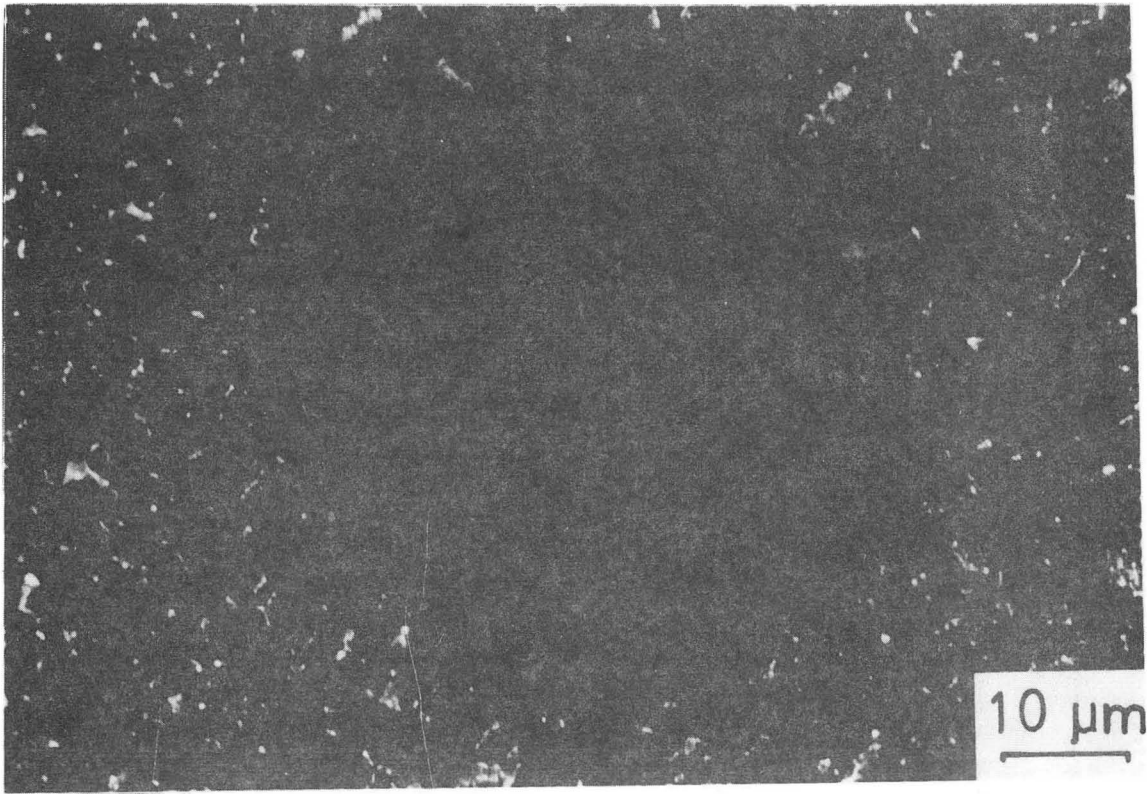


30 μm

XBB 858-6469

\downarrow σ_{∞}

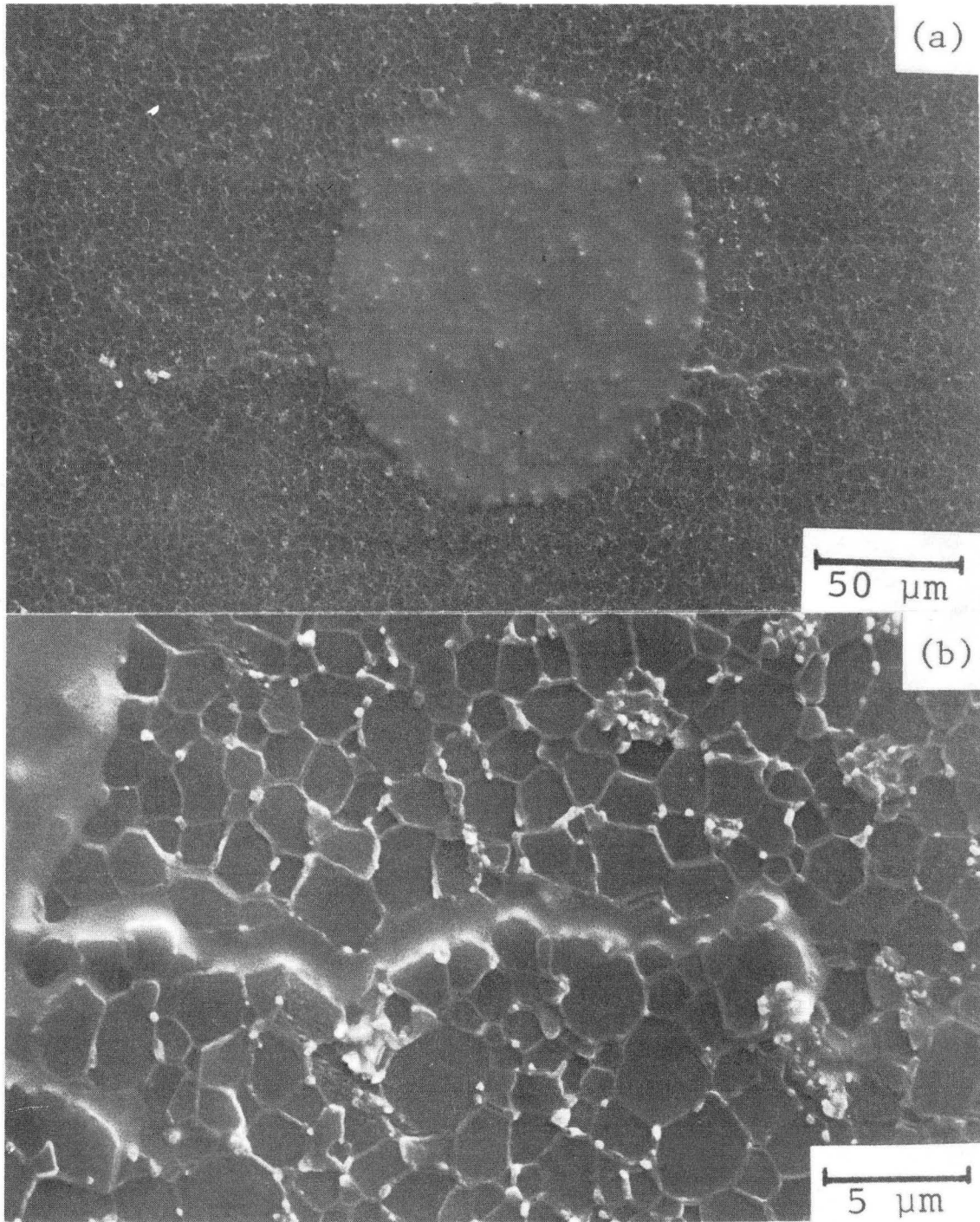
Fig. 1



XBB 857-5878

Fig. 2

↑ σ_{∞}



XBB 854-3091

Fig. 3

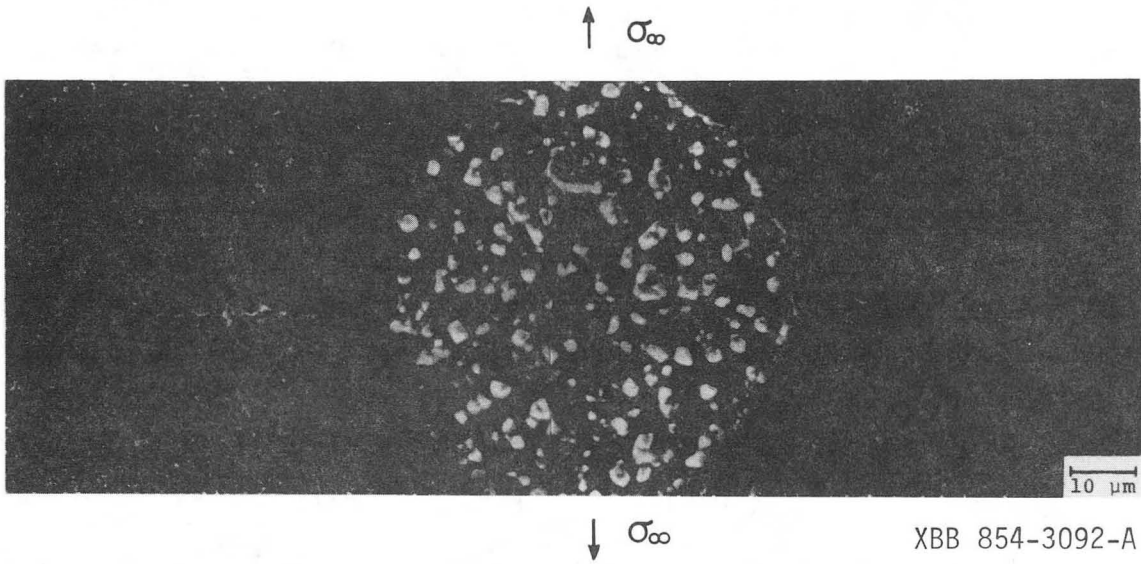
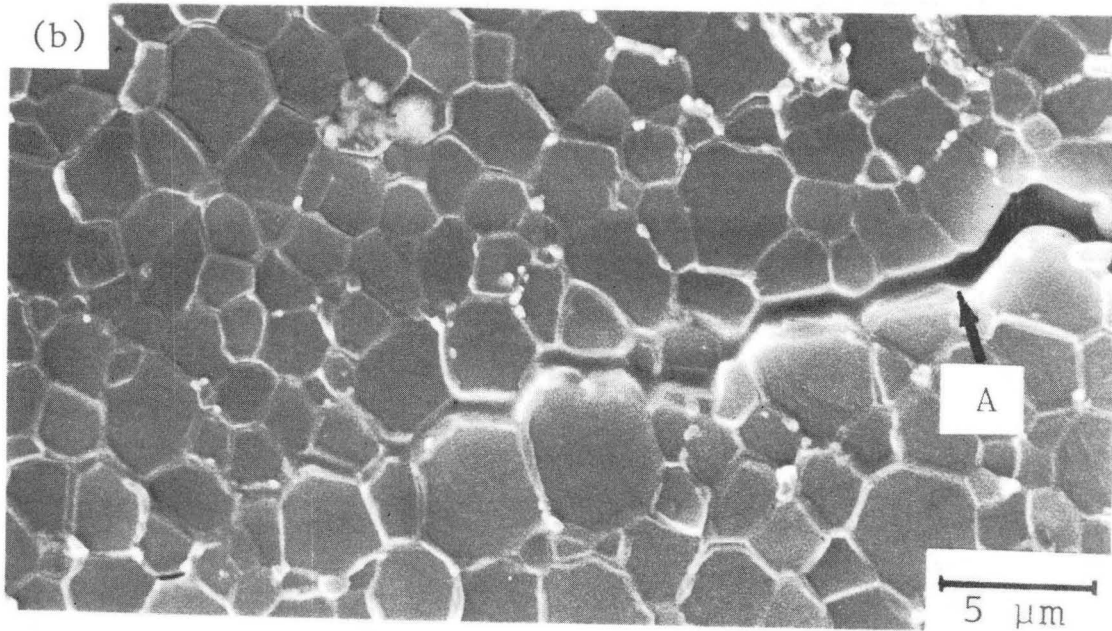
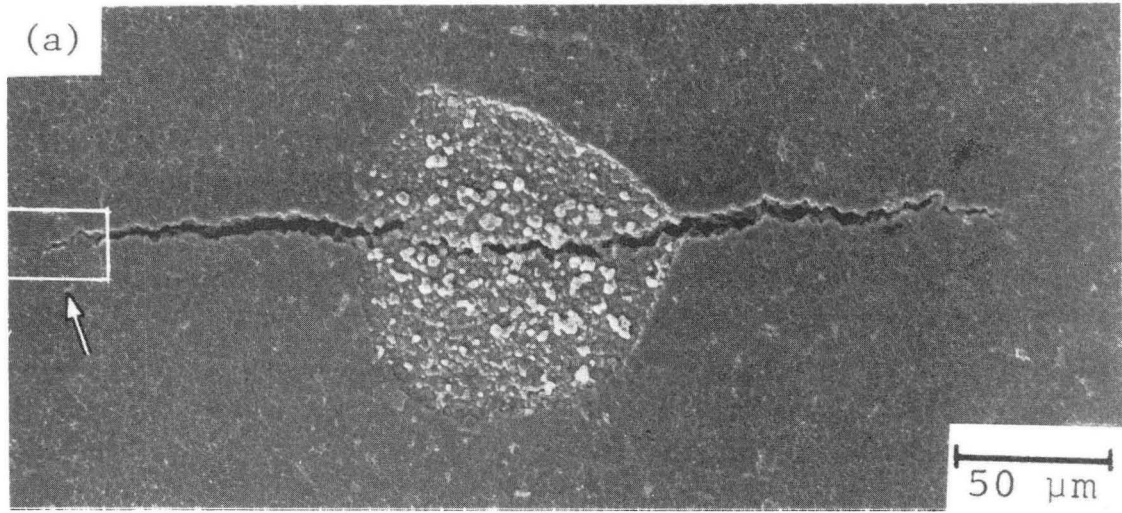


Fig. 4

29

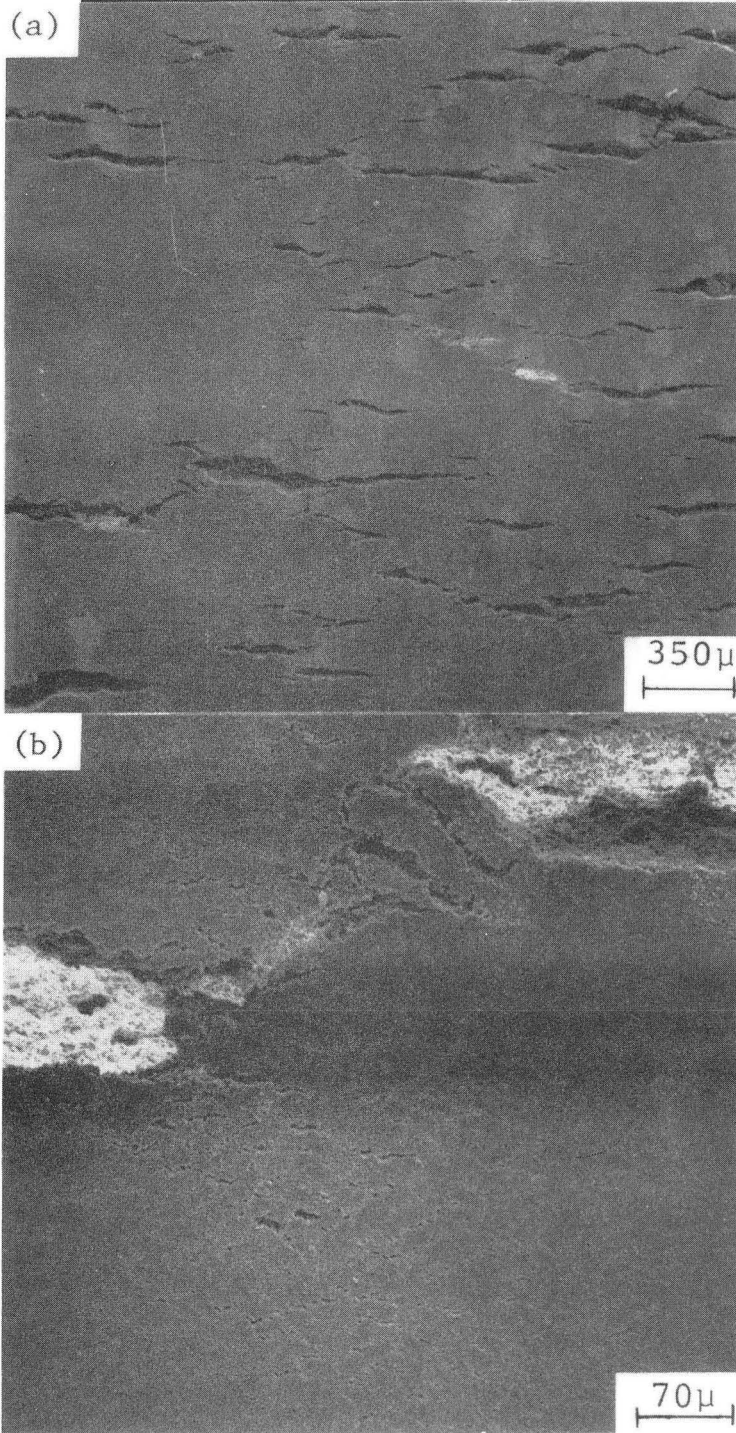
↑ σ_{∞}



XBB 854-3093-A

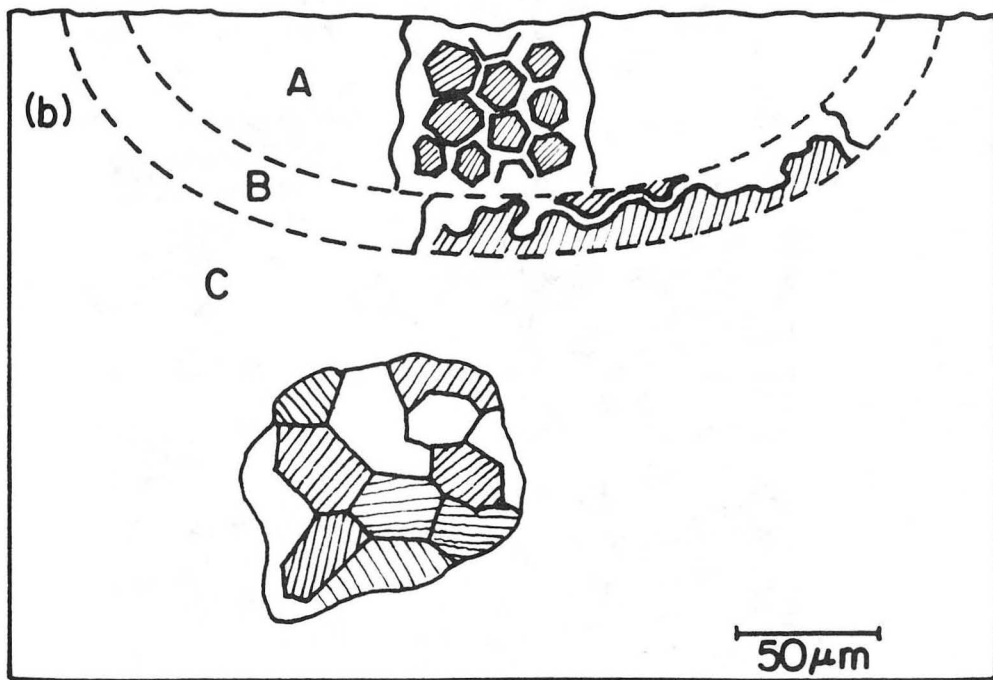
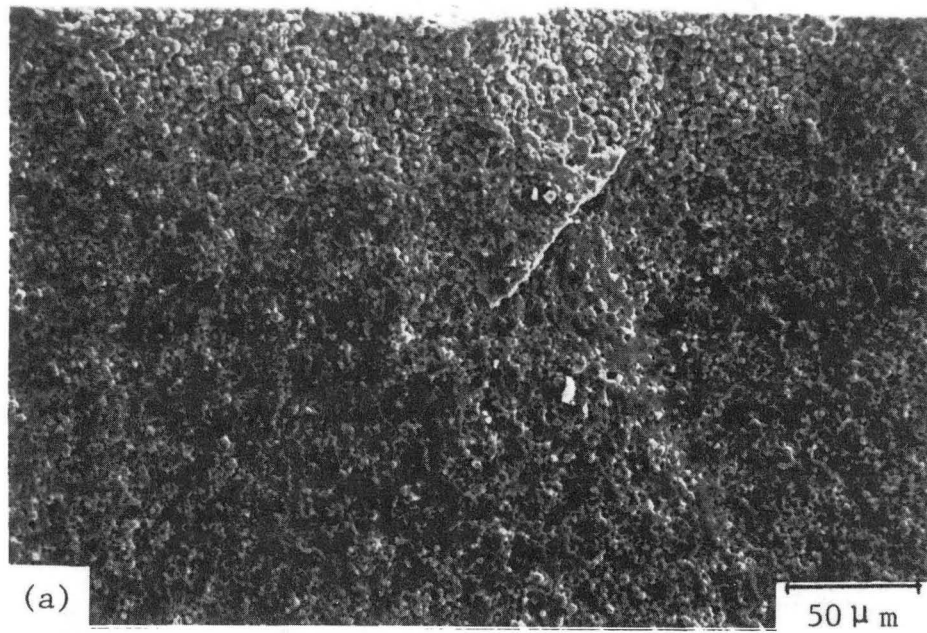
Fig. 5

30



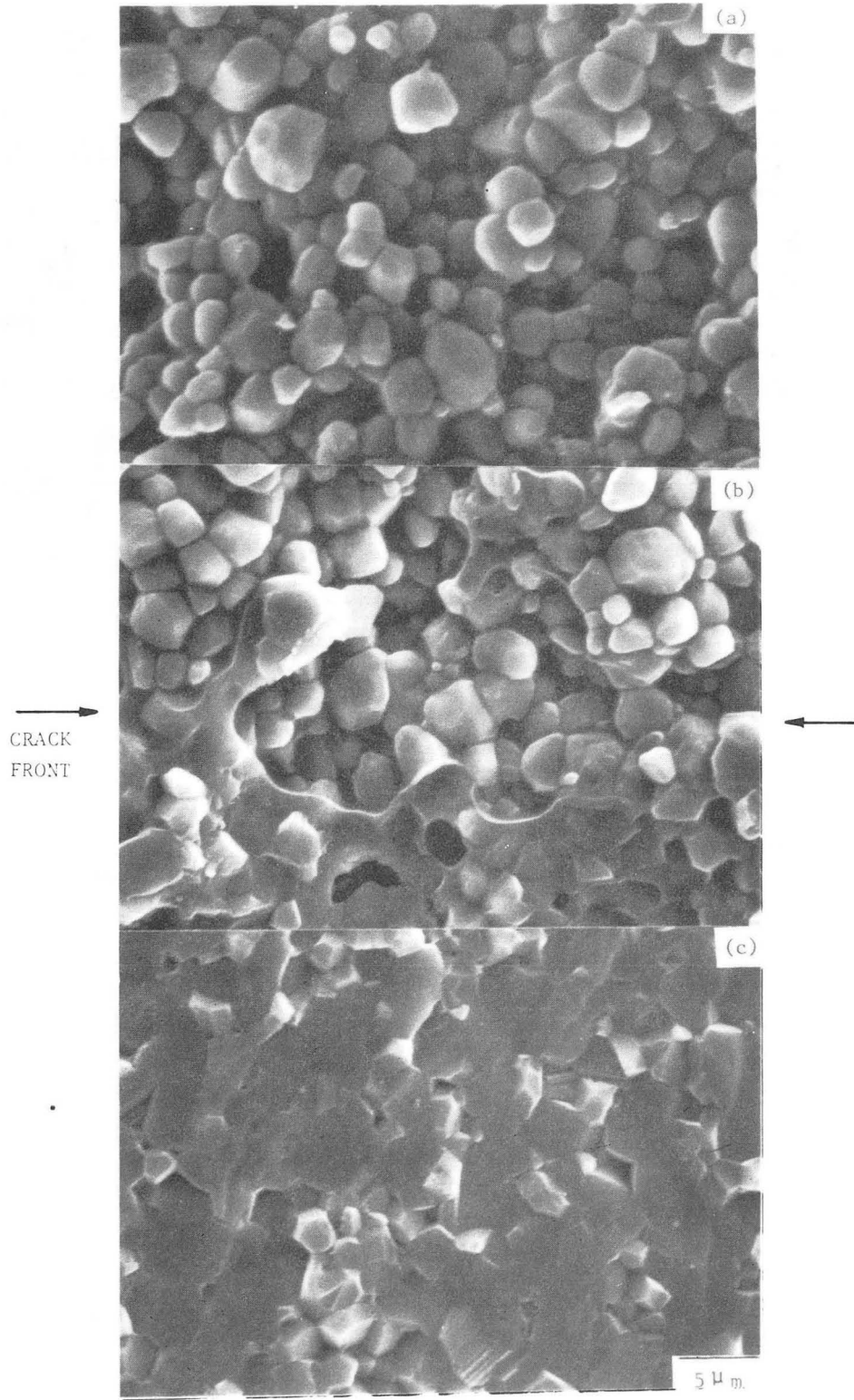
XBB 857-5879-A

Fig. 6



XBB 857-5880

Fig. 7



XBB 854-3087

Fig. 8

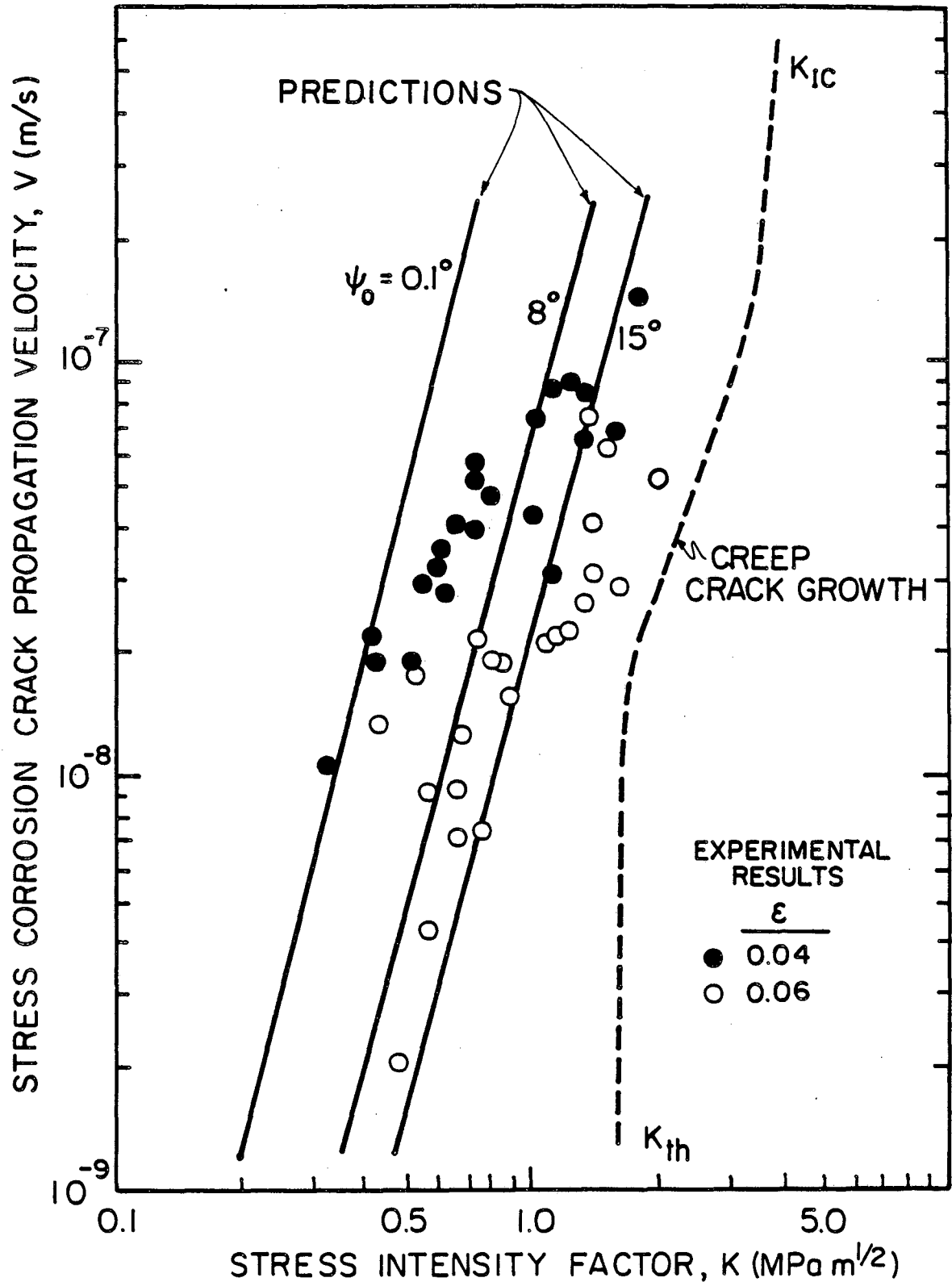
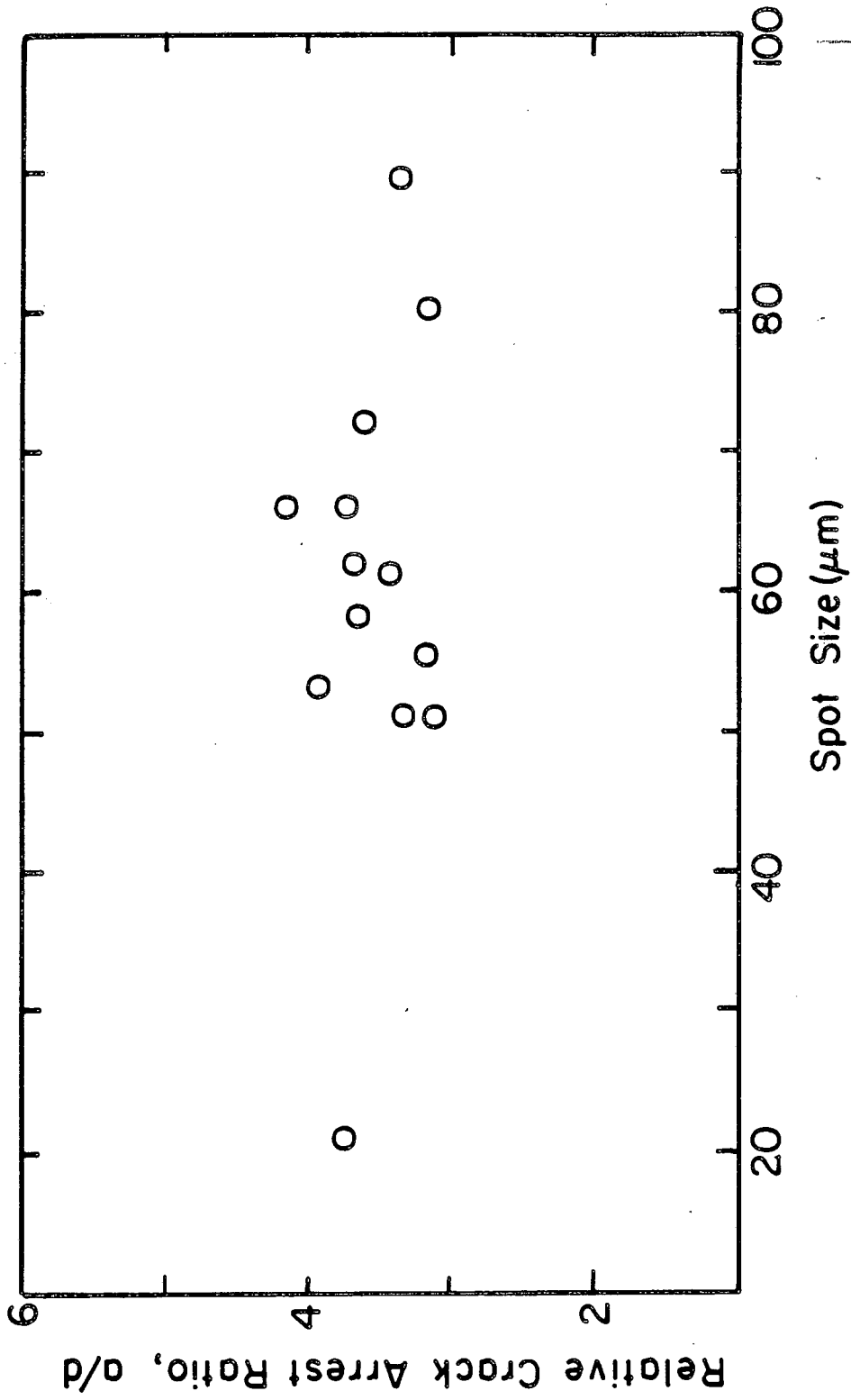


Fig. 9

XBL 859-3830



XBL858-6536

Fig. 10

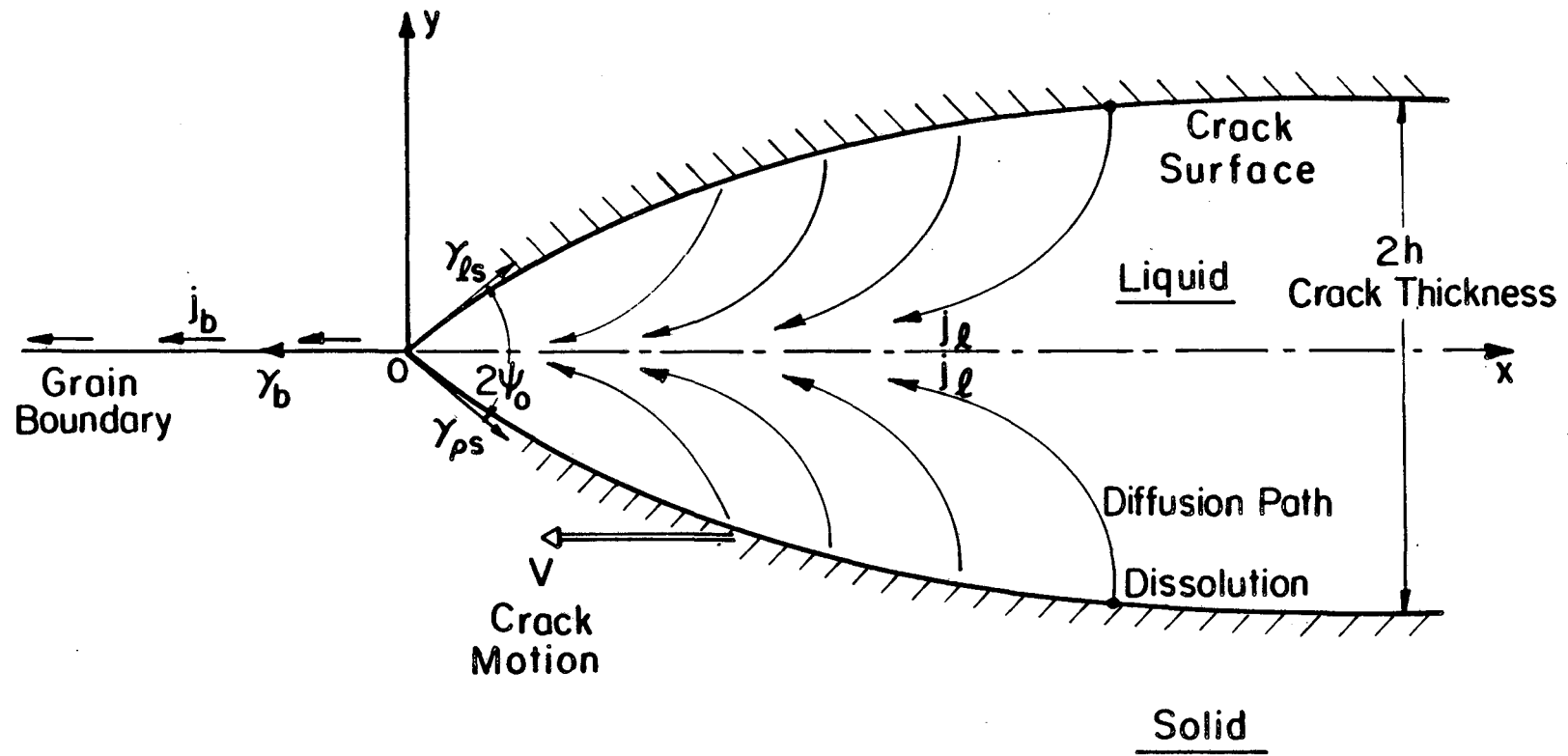
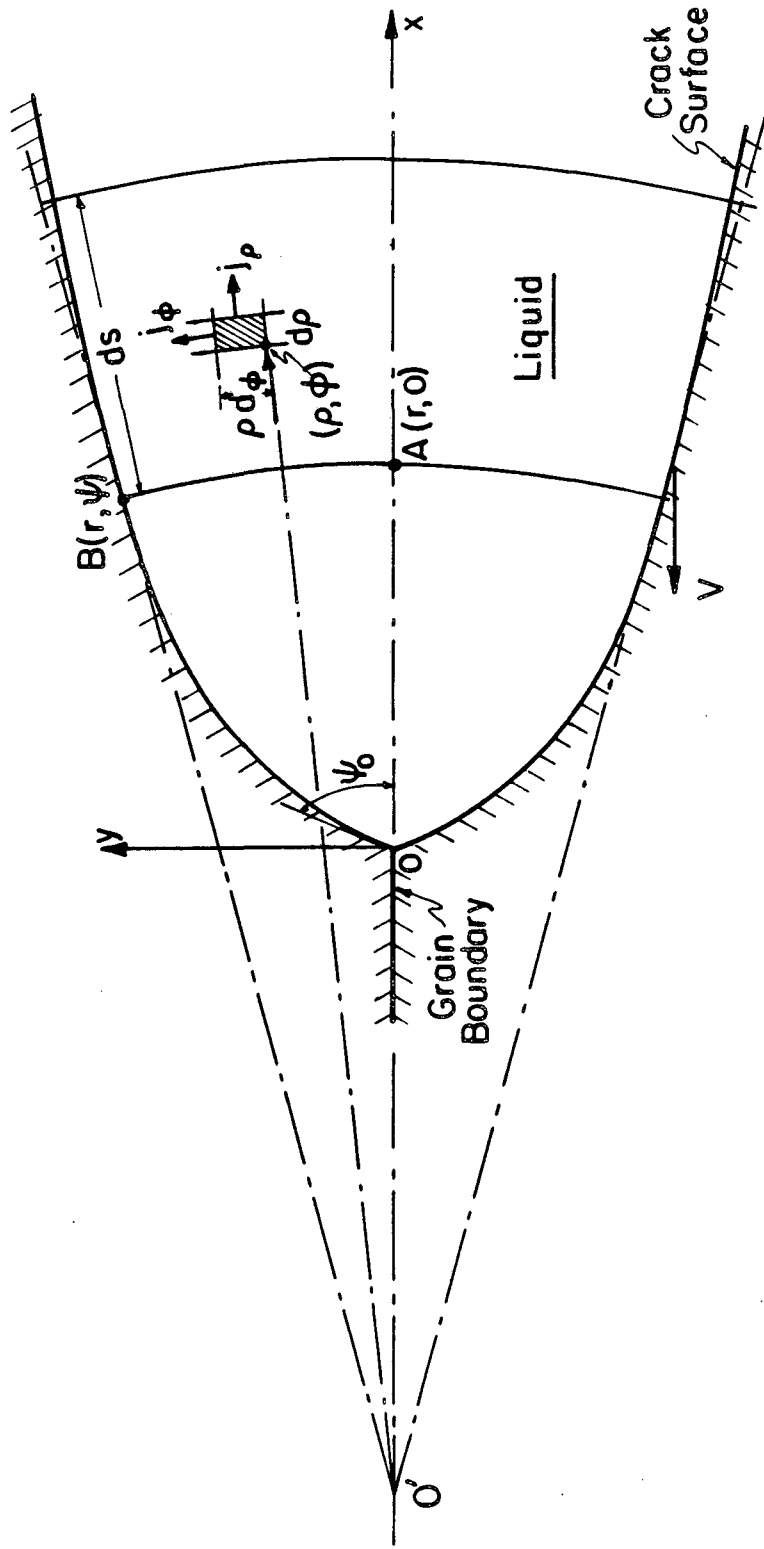


Fig. 11a

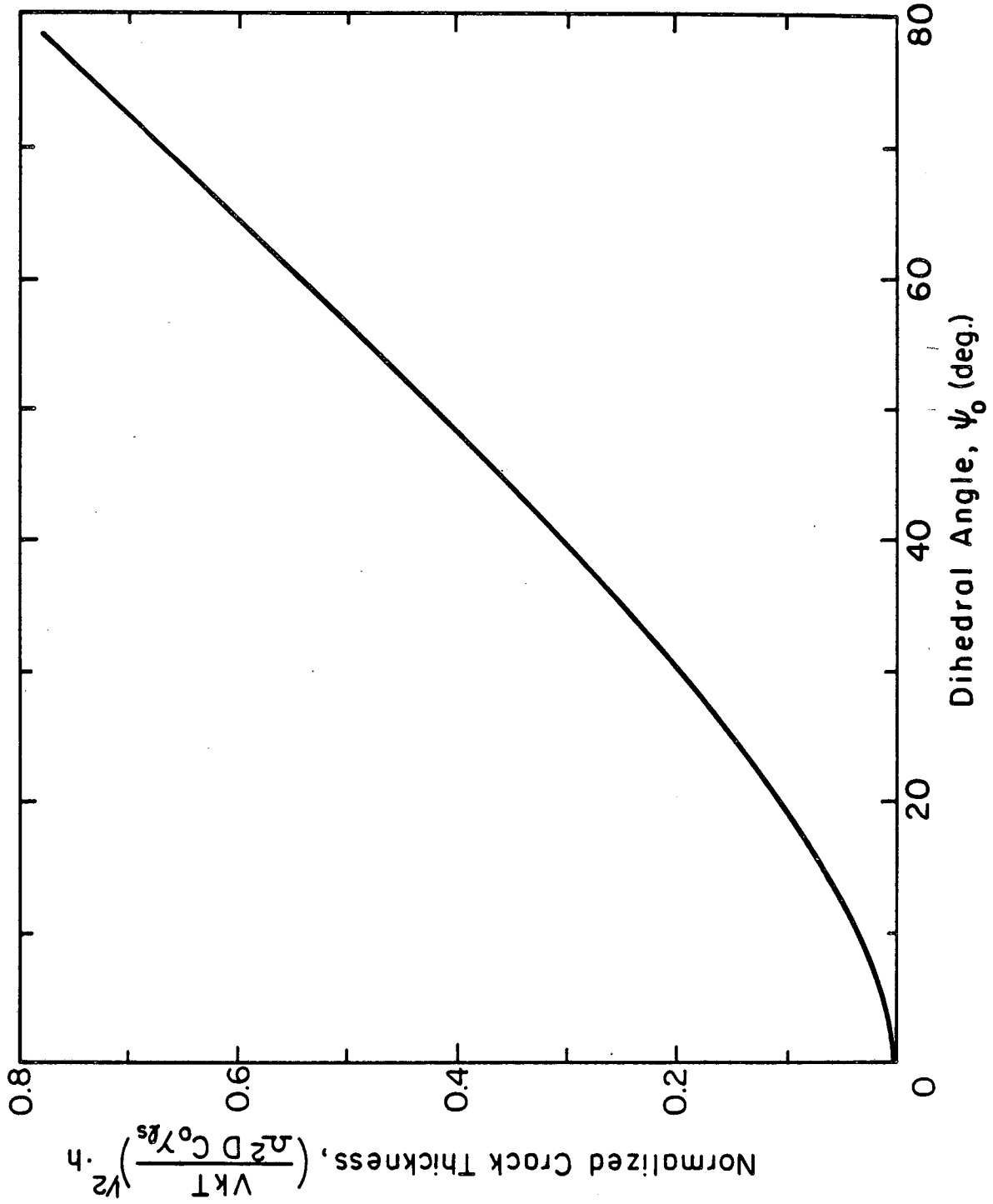
XBL 858-6537



Solid

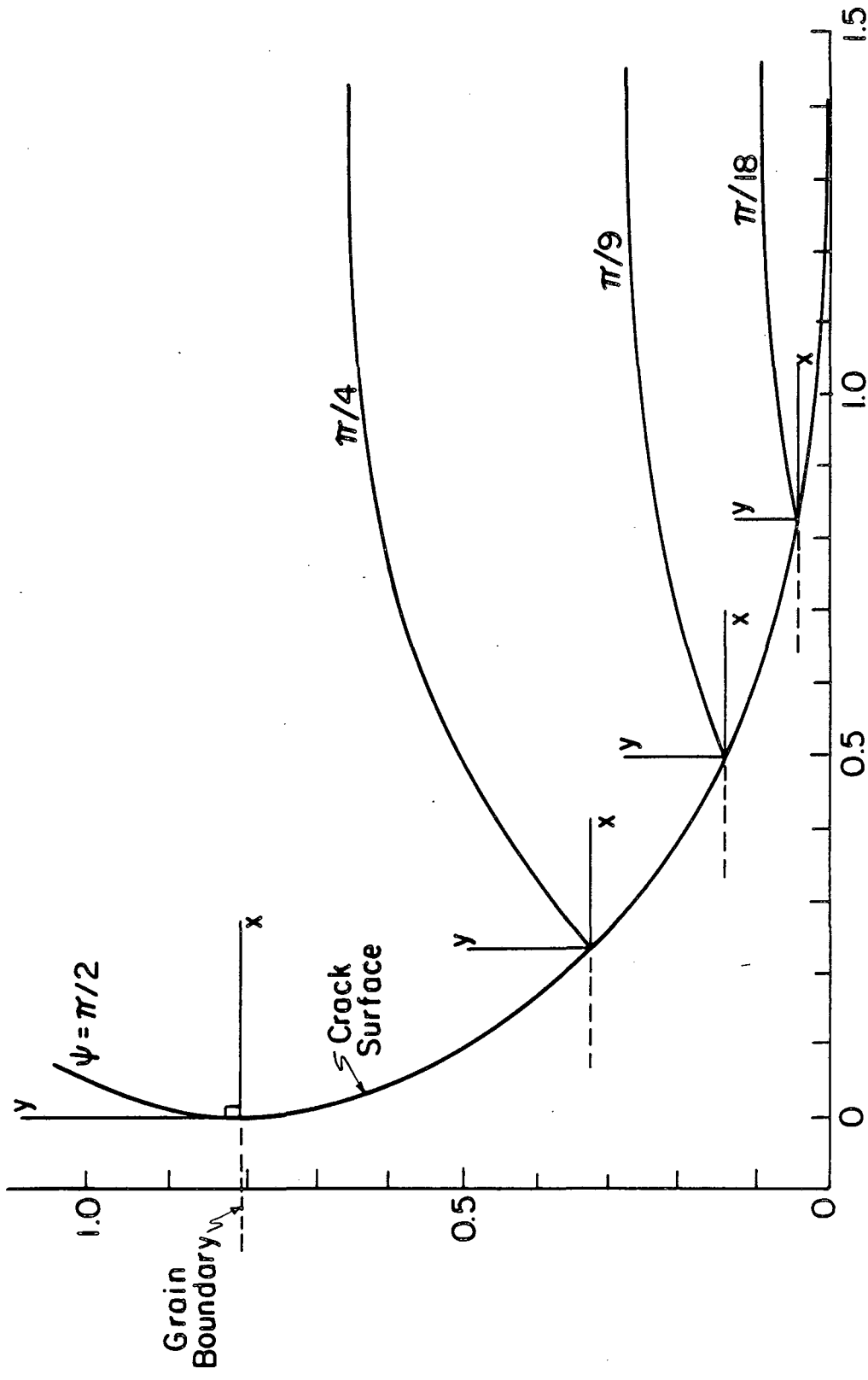
XBL 858-6-538

Fig. 11b



XBL 858-6540

Fig. 12



XBL 858-6539

Fig. 13

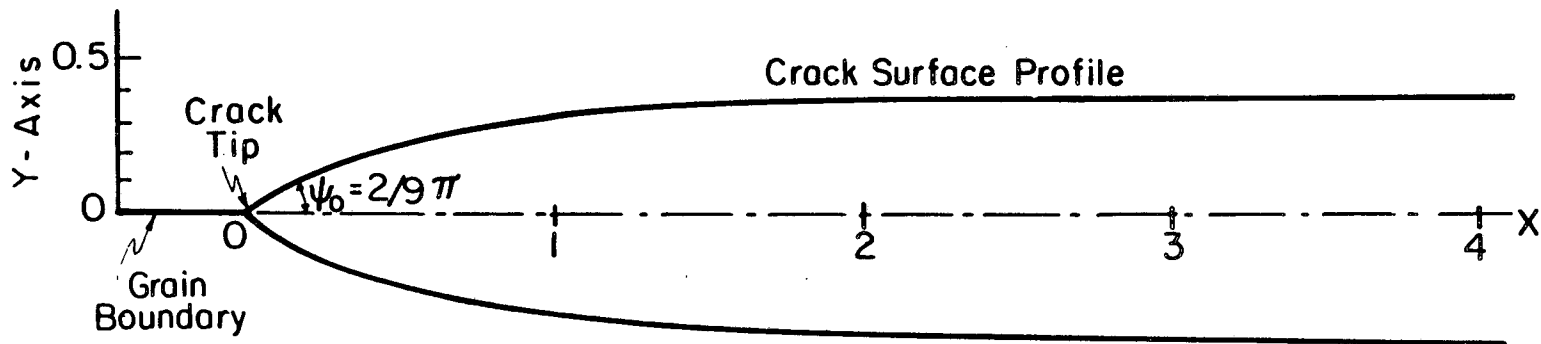
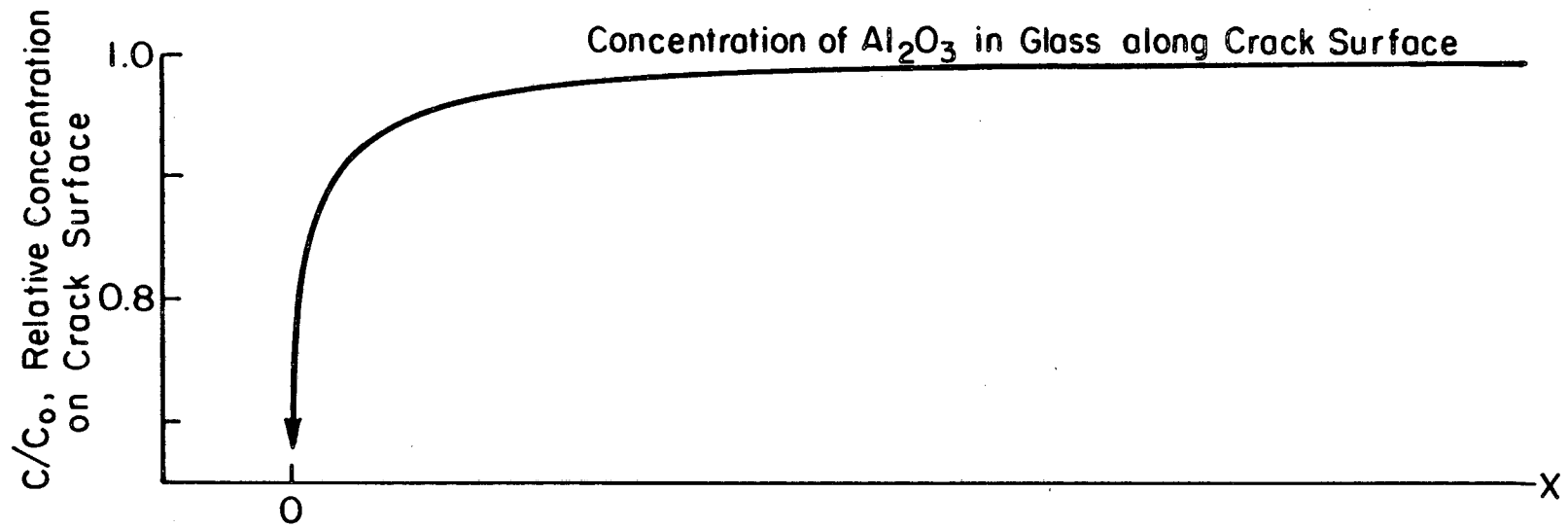


Fig. 14

XBL 858-6541

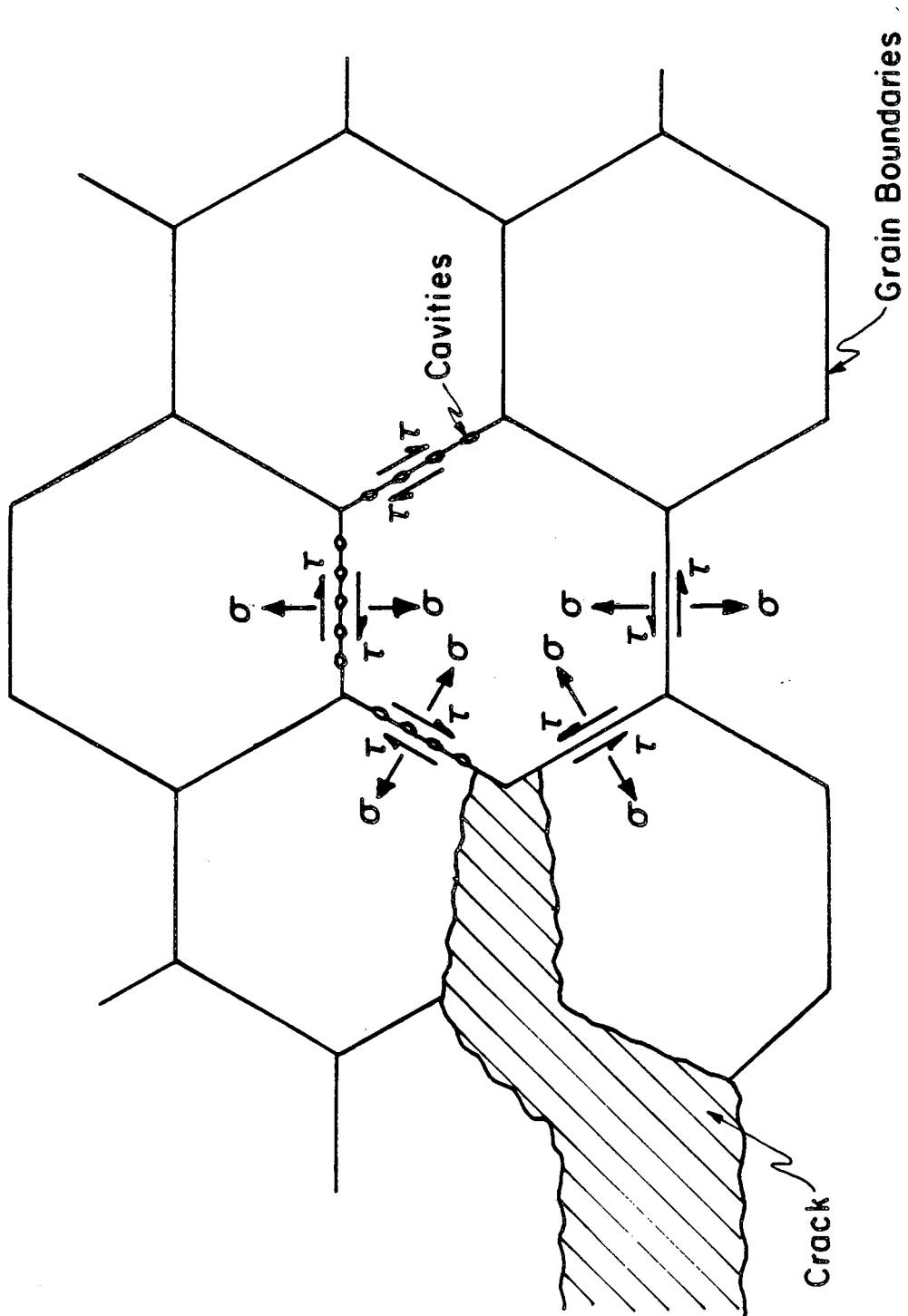
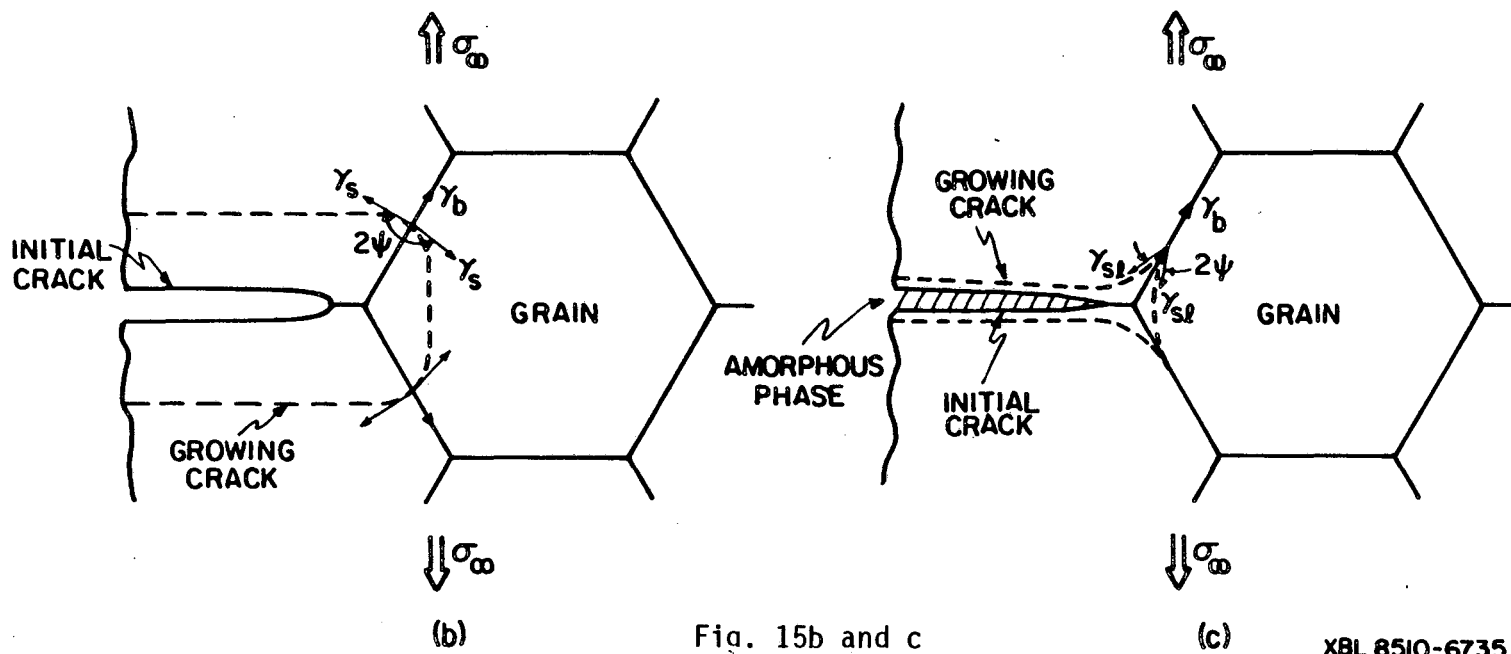


Fig. 15a

XBL 832-5229



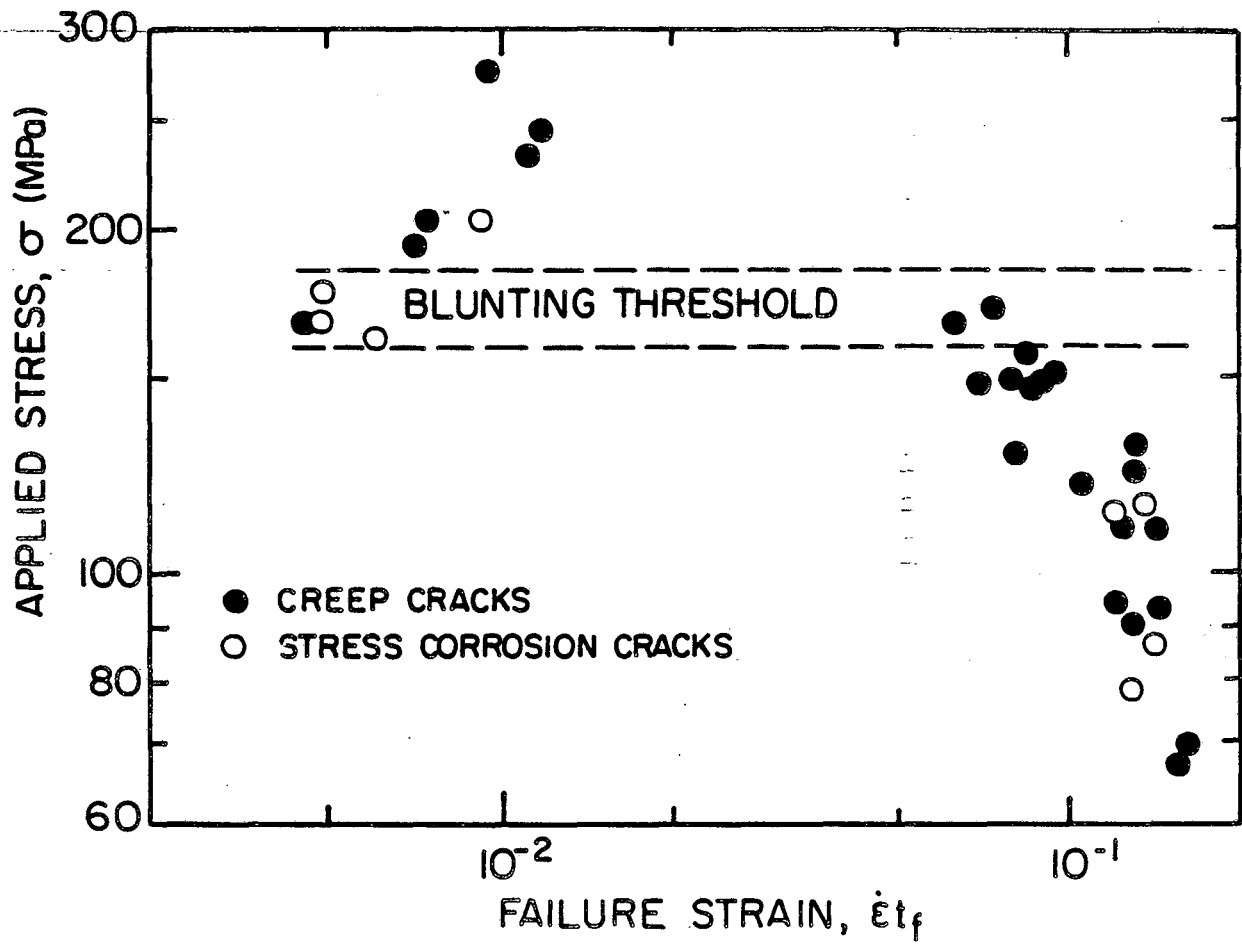


Fig. 16

XBL 8510-6733

This report was done with support from the Department of Energy. Any conclusions or opinions expressed in this report represent solely those of the author(s) and not necessarily those of The Regents of the University of California, the Lawrence Berkeley Laboratory or the Department of Energy.

Reference to a company or product name does not imply approval or recommendation of the product by the University of California or the U.S. Department of Energy to the exclusion of others that may be suitable.

TECHNICAL INFORMATION DEPARTMENT
LAWRENCE BERKELEY LABORATORY
UNIVERSITY OF CALIFORNIA
BERKELEY, CALIFORNIA 94720